This article has been accepted for publication in a future issue of this journal, but has not been fully edited. Content may change prior to final publication. Citation information: DOI 10.1109/TBCAS.2019.2917690, IEEE Transactions on Biomedical Circuits and Systems

An Energy Efficient Multi-User Asynchronous Wireless Transmitter for Biomedical Signal Acquisition

Tomislav Matić, *Member, IEEE*, Leon Šneler and Marijan Herceg, *Member, IEEE*

***Abstract*—The paper presents a novel transmitter architecture for short-range asynchronous wireless communication, applicable to simultaneous multi-user wireless acquisition of biological signals. The analog signal, provided from an analog biosensor, is transformed to time information using an Integral Pulse Frequency Modulator (IPFM) as a Time-Encoding Machine (TEM). The IPFM generates a time-encoded unipolar pulse train, maintaining the linear dependence of the output pulse distance on analog input voltage. The system enables continuous acquisition of the signals from multiple sensors in which each transmitter has unique feedback loop delay used for multi-user coding. IPFM pulses trigger the Impulse Radio Ultra-Wideband (IR-UWB) pulse generator directly, providing two Ultra-Wideband (UWB) pulses per each IPFM pulse. Due to the lack of internal clock signal and microprocessor-free multi-user coding, the circuitry satisfies the requirements of multi-user coding energy efficiency and size reduction, which are crucial demands in biomedical applications. The proposed Time-Encoded UWB (TE-UWB) transmitter is implemented in $0.18\ \mu$m CMOS technology. Measurement results of the IPFM transfer function for input voltage ranging from 0.15 V to 1.5 V are presented, providing the dependence of the IPFM pulse time distance on analog input voltage and power consumption dependence on the input voltage level. For continuous monitoring operation total power consumption of the transmitter circuitry for the maximum input voltage is $10.8\ \mu$W, while for the lowest input voltage it increases to $40.48\ \mu$W. The circuit occupies $0.14\ \text{mm}^2$.**

***Index Terms*—Wireless communication, Ultra wideband technology, Pulse modulation, Time encoding, Asynchronous communication, Body sensor networks, Biosensors.**

I. Introduction

ULTRA-Wideband (UWB) technology has emerged as a promising solution for wireless communication and monitoring in biomedical applications [1]–[6]. Due to low energy consumption, wide bandwidth and low power spectral density (PSD), UWB technology provides crucial benefits for wireless communication within Body Area Networks (BAN), Personal Area Networks (PAN), wearable devices and biomedical implants. Besides wireless communication and monitoring in biomedical applications, UWB is widely used in the impulse radio localization and radar systems [7]–[9] due to the robustness in interferer-intense environments with a low level of spectral density.

This work is supported in part by the Croatian Science Foundation under the project UIP-2014-09-6219 "Energy efficient asynchronous wireless transmission" and Europractice MPW and design tool support stimulation program First IC design. Tomislav Matić, Leon Šneler and Marijan Herceg are with the Department of Communications, Faculty of Electrical Engineering, Computer Science and Information Technology, Osijek, Croatia. (e-mail addresses: tomislav.matic@ferit.hr, leon.sneler@ferit.hr, marijan.herceg@ferit.hr).

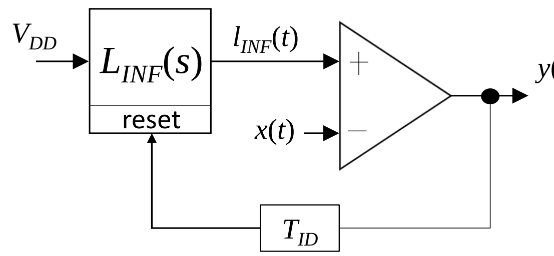

Fig. 1: Generalized block scheme of the proposed IPFM.

A rising number of wearable devices in BANs and PANs for healthcare [10]–[12] and sport activity tracking [13], [14] requires a high number of connected sensors within short distance. The most common solutions for wireless connectivity within PAN and BAN systems use Bluetooth Low Energy (BLE) modules [15], ZigBee [16], ANT [10] or similar devices, operating at 2.4 GHz. Impulse-Radio UWB (IR-UWB) wireless transmission is becoming more attractive for low power short-range wireless applications due to low energy per transmitted pulse and wide spectrum utilization. Besides energy efficiency demands, an increasing number of connected IoT devices requires novel solutions for wireless connectivity due to increasing spectrum congestion at the 2.4 GHz frequency band. The wideband power spectrum of UWB pulses enables higher spectrum utilization and lower spectrum congestion. Besides spectrum congestion issues, energy efficiency of BLE is achieved by using low duty-cycling operation [17], which is critical for constant monitoring applications. Duty-cycling operation is applicable in biomedical wireless sensors for measurement of slowly varying parameters, like body temperature measurement, intracranial and intraocular pressure monitoring [18], [19], physiological signals of the human gastrointestinal tract, pH level [20] or blood glucose concentration monitoring [21]. Blood glucose monitor, reported in [21] reports self-powered wireless physiochemical sensing system for monitoring of glucose or lactate in bodily fluids consuming average power equal to $1.15\ \mu$W. Besides low duty-cycling ratio (1 %) used for periodic activation of RF transmitter, low operating voltage equal to 0.3 V additionally contributes to energy efficiency of the system.

Duty cycling operation can also be used in RF transmitters for measurement of biomedical signals with higher frequency range, like ECG measurement in [22], which however requires integration of memory in transmitter and higher hardware complexity. Therefore, due to its low circuit complexity and

This article has been accepted for publication in a future issue of this journal, but has not been fully edited. Content may change prior to final publication. Citation information: DOI 10.1109/TBCAS.2019.2917690, IEEE Transactions on Biomedical Circuits and Systems

low power consumption at high data rates, UWB systems provide energy efficient solution for constant monitoring applications and measurement of fast varying biological signals, like Action potential, ECG, EEG, EMG and ENG signals [23]. As a promising alternative for Bluetooth and similar competing technologies in numerous application areas, UWB is becoming efficients solution for wireless communication, particularly in BANs [24], which is defined in the IEEE 802.15.6 standard for Wireless Body Area Networks (WBAN). Application of UWB transmitters with clockless acquisition of biomedical signal additionally contributes to energy efficiency [6]. Wireless ECG SoC for wearable applications reported in [6] consumes power equal to 2.89 μW for 150 Hz input signal frequency range. The proposed Asynchronous Level-Crossing Analog-to-Digital Converter (LC-ADC) architecture in [6] provides low power operation, but it is applicable for low input signal frequency range.

This paper presents the TE-UWB transmitter integrated circuit suitable for biomedical wireless sensing applications, providing multi-sensor communication with no internal clock signal or microprocessor, applicable in BAN. The proposed time-encoding transmitter architecture based on TEM and IR-UWB provides energy efficient multi-user constant monitoring which is crucial in healthcare applications, where continuous transmission is required. Without applying the UWB pulse shaper, the IPFM modulator based transmitter architecture also enables simple implementation of the multi-sensor communication network in human body communications (HBC). The proposed energy efficient multi-user asynchronous wireless transmitter for biological signal acquisition employs IPFM based analog-to-time conversion and a delay line for multi-user coding. The analog input signal acquired from an analog biosensor is applied to the IPFM, which transforms an analog signal to time information conveyed in the time distance between two consecutive output pulses. A similar approach is used for sensor-to-time conversion in [25] for single sensor wireless communication. However, this paper presents an architecture suitable for multi-sensor signal acquisition. For implementation of the multi-user network, each transmitter within the network has a unique IPFM feedback loop delay denoted as sensor ID T_{ID}, which is used for user coding at the transmitter side and for user decoding at the receiver side.

This paper is organized as follows: In Section II, Integral Pulse Frequency Modulation is described providing the analysis of the IPFM parameters for accurate time encoding and multi-user coding. Section III describes TE-UWB transmitter implementation including the transmitter circuit description. Simulation and measurement results are presented in Section IV including the comparison with the state-of-the-art UWB transmitters and Section V gives concluding remarks.

II. Multi-User Integral Pulse Frequency Modulation

The concept of TEMs was firsty introduced by Lazar and Toth [26]. Possible implementations of TEM include Asynchronous Sigma-Delta Modulator (ASDM) [26], [27], Integrate and Fire (IAF) [26] circuit or IPFM [28]–[32]. The proposed transmitter architecture is based on the IPFM circuit, which performs analog input voltage to output pulse frequency conversion. The IPFM circuit enables implementation of the simple multi-user scheme which can be implemented using feedback loop delay to encode the particular user and enable multi-user detection at the receiver side.

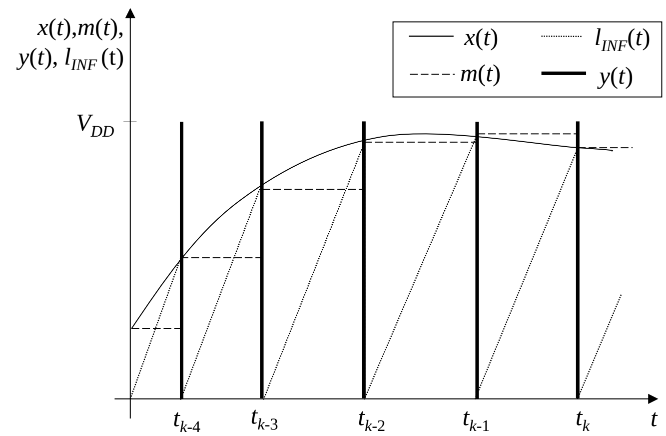

Fig. 2: Corresponding waveforms of the IPFM from the Fig. 1 for $T_{ID} = 0$.

A. IPFM Time Encoding

The block scheme in Fig. 1 represents an ideal IPFM with zero feedback loop delay ($T_{ID} = 0$). The basic principle of the IPFM is shown in Fig. 2. In particular, the waveforms in Fig. 2 represent the provisional analog input signal $x(t)$ (solid line curve in Fig. 2), the integrator output signal $l_{INF}(t)$ (dotted line in Fig. 2), the modulated signal $m(t)$ (dashed line in Fig. 2, continuous value between two consecutive pulses $y(t)$) and the IPFM output signal $y(t)$ (bold solid line) for an ideal IPFM with $T_{ID} = 0$, which presents a single-user scenario. The modulated signal $m(t)$ represents the sampled information of the analog input signal stored into the time distance between two consecutive preceding IPFM output pulses. The analog IPFM input voltage $x(t)$ is applied to the comparator inverting input, while the integrator is fed by constant voltage V_{DD}. Due to constant integrator input voltage, the slope of the integrator output signal $l_{INF}(t)$ is constant. The IPFM output signal $y(t)$ is a rectangular pulse train with time distance between the two consecutive pulses proportional to the analog input signal $x(t)$. During the time interval between two consecutive IPFM output pulses $[t_{k-1}, t_k]$, the integrator will produce an output ramp with a constant slope. The amplitude of the ramp at the moment t_k depends on the analog input signal value $x(t_k)$. If the output signal of the integrator at the moment t_{k-1} is equal to 0, the amplitude of the ramp $l_{INF}(t_k)$ at the moment t_k is equal to:

$$l_{INF}(t_k) = \int_{t_{k-1}}^{t_k} \frac{V_{DD}}{\tau_{INF}} dt = \frac{V_{DD}}{\tau_{INF}} (t_k - t_{k-1}) = x(t_k), \quad (1)$$

where τ_{INF} is $L_{INF}(s)$ integrators time constant.

This article has been accepted for publication in a future issue of this journal, but has not been fully edited. Content may change prior to final publication. Citation information: DOI 10.1109/TBCAS.2019.2917690, IEEE Transactions on Biomedical Circuits and Systems

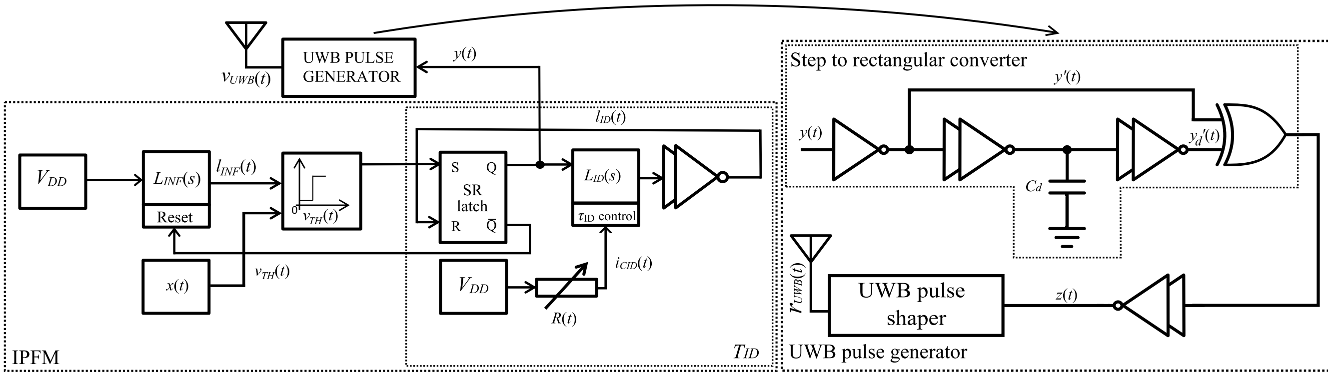

Fig. 3: Block scheme of the Time Encoding Ultra-Wideband transmitter and the UWB pulse generator.

According to (1), the time distance between two consecutive IPFM output pulses is proportional to the analog input signal:

$$t_k - t_{k-1} = \frac{\tau_{INF}}{V_{DD}} x(t_k). \tag{2}$$

To satisfy the condition for successful voltage to time conversion, the absolute value of the $L_{INF}(s)$ integrator output derivation has to be much higher than the maximum absolute value of the input signal derivation $\frac{dx(t)}{dt}$. Therefore, the analog input signal has to be band limited. Accordingly, for sinusoidal input signals, the maximum analog input signal frequency should be limited to satisfy the following criterion:

$$1/\tau_{INF} >> \max(|\frac{dx(t)}{dt}|). \tag{3}$$

An analog to time conversion error is defined as the difference of the input signal $x(t)$ and the modulated signal $m(t)$:

$$\varepsilon = x(t) - m(t). \tag{4}$$

The modulated signal $m(t)$ is constant within the interval between two consecutive pulses. As shown in Fig. 2, its value is equal to the input signal value $x(t)$ at the beginning of the interval between two consecutive pulses. Therefore, in the interval $[t_k, t_{k-1}\rangle$ the modulated signal is equal to:

$$m(t) = x(t_{k-1}), t \in [t_{k-1}, t_k\rangle. \tag{5}$$

The accumulated error ε_k in the interval $[t_k, t_{k-1}\rangle$ is equal to the integral of the difference $x(t) - m(t)$:

$$\varepsilon_k = \int\limits_{t_{k-1}}^{t} [x(t) - m(t)]dt = \int\limits_{t_{k-1}}^{t} [x(t) - x(t_{k-1})]dt. \tag{6}$$

It should be emphasised that the general block scheme in Fig.1 is suitable only for unipolar analog input signals. For bipolar input signals, an input signal has to be shifted to the positive range between 0 and V_{DD} voltage. In that way, a sinusoidal input signal $x(t) = V_{DD}\sin(\omega t)$ applied to inverting comparator input becomes:

$$x(t) = \frac{V_{DD}}{2} + \frac{V_{DD}}{2}\sin(\omega t) \tag{7}$$

and the accumulated error ε_k is equal to:

$$\begin{aligned}\varepsilon_k = &\frac{V_{DD}}{2\omega}\left[\cos(\omega t_{k-1}) - \cos(\omega t_k)\right] \\ &- \frac{V_{DD}}{2}\sin(\omega t_{k-1})(t_k - t_{k-1}).\end{aligned} \tag{8}$$

According to (2) and (8), the accumulated error ε_k is equal to:

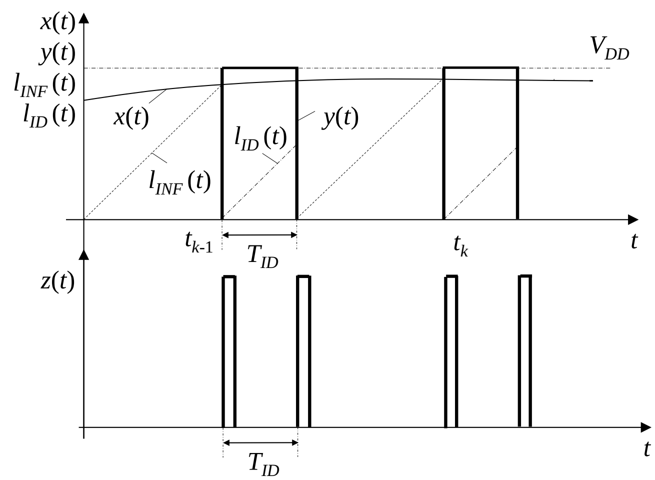

Fig. 4: Corresponding waveforms of the IPFM from the Fig. 3 for $T_{ID} > 0$.

$$\begin{aligned}\varepsilon_k = &\frac{V_{DD}}{2\omega}\left[\cos(\omega t_{k-1}) - \cos(\omega t_k)\right] \\ &-\sin(\omega t_{k-1})\frac{V_{DD}\tau_{INF}(2-\cos(\omega t_k))}{4} \\ = &\frac{V_{DD}}{4\omega}\left[2\cos(\omega t_{k-1}) - 2\cos(\omega t_k)\right. \\ &\left.-\omega\tau_{INF}\sin(\omega t_{k-1})(2-\cos(\omega t_k))\right].\end{aligned} \tag{9}$$

If the integrator gain $1/\tau_{INF} >> \omega$ and $2\cos(\omega t_{k-1}) - 2\cos(\omega t_k) \approx 0$ then $\omega\tau_{INF} << 1$. Therefore, according to equation (9), $\varepsilon_k \approx 0$.

This article has been accepted for publication in a future issue of this journal, but has not been fully edited. Content may change prior to final publication. Citation information: DOI 10.1109/TBCAS.2019.2917690, IEEE Transactions on Biomedical Circuits and Systems

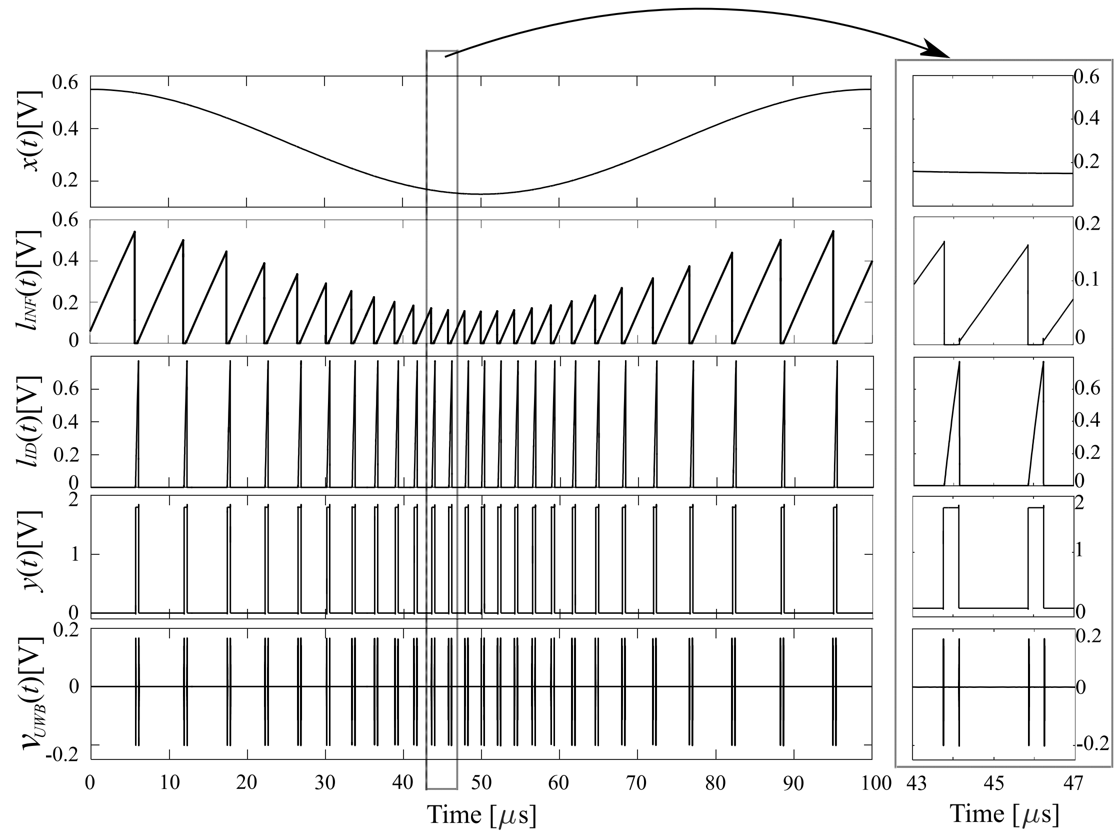

Fig. 5: The corresponding TE-UWB transmitter waveforms for the input signal $x(t) = 0.35 + 0.2sin(6.28 \times 10^4 t)$ with $T_{ID} = 383.25\ ns$

B. Multi-User Scheme

The proposed TE-UWB transmitter block scheme is depicted in Fig. 3, including the IPFM circuit and the UWB pulse generator. The analog input voltage $x(t)$ is applied to the inverting comparator input, while the $L_{INF}(s)$ constant slope integrator is applied to the non-inverting comparator input. The comparator is followed by the SR latch, which drives the $L_{ID}(s)$ integrator used for multi-user coding. Each user has an unique sensor ID T_{ID}, which is defined by the $L_{ID}(s)$ integrator time constant τ_{ID}. The IPFM output pulse train $y(t)$ is fed to the UWB pulse generator. The UWB pulse generator consists of a Step to rectangular pulse converter and a UWB pulse shaper. The Step to rectangular pulse converter is implemented by using the delay circuit which consists of two inverter gates and capacitor C_d. The input signal $y'(t)$ and the output signal $y'_d(t)$ of the delay circuit are fed into the EX-OR logic gate. For each rising or falling edge of the signal $y(t)$, the positive rectangular pulse $z(t)$ is formed at the output of the step to rectangular converter and its width is determined by the propagation delay of the inverter logic gate and the value of capacitor C_d. For each $z(t)$ pulse, one UWB pulse is generated at the output of the UWB pulse shaper.

Fig. 4 provides an example of the corresponding IPFM waveforms $x(t)$, $y(t)$, $l_{INF}(t)$, $l_{ID}(t)$ and $z(t)$ for the provisional analog input voltage $x(t)$. The constant input voltage V_{DD} is applied to the input of the integrator $L_{INF}(s)$. Accordingly, the $L_{INF}(s)$ integrator output slope remains constant independently of the analog input voltage $x(t)$. At the moment when $l_{INF}(t)$ reaches the value equal to the analog input voltage $x(t) = v_{TH}(t)$, the comparator changes the output from zero voltage to V_{DD}. Once the comparator is triggered, the integrator $L_{ID}(s)$ starts integrating until it reaches the inverter buffer threshold voltage ($l_{ID}(t)$=$V_{DD}/2$). The width of the formed pulse $y(t)$ is equal to T_{ID} and it represents the sensor ID, which is used for particular sensor coding and decoding at the receiver side. The sensor ID is defined by $L_{ID}(s)$ integrator time constant τ_{ID}, which defines the integrator output slope and therefore the duration of the IPFM pulse. Including the sensor ID T_{ID}, the time distance between occurrence of the two consecutive IPFM output pulses t_k and t_{k-1} of the signal $y(t)$ is equal to:

$$\begin{aligned} t_k - t_{k-1} &= \frac{\tau_{INF}}{V_{DD}} x(t_k) + T_{ID} \\ &= \frac{\tau_{INF}}{V_{DD}} x(t_k) + \frac{\tau_{ID}}{2}. \end{aligned} \tag{10}$$

If the integrator time constant τ_{INF} and the sensor ID T_{ID} are known on the receiver side, according to (10), it is simple to demodulate the pulse train and obtain the analog input voltage value $x(t_k)$. In multi-user systems, each user has unique T_{ID}. Different sensor ID delay values for the m-th and the n-th user T_{IDm} and T_{IDn} enable particular user decoding on the receiver side.

This article has been accepted for publication in a future issue of this journal, but has not been fully edited. Content may change prior to final publication. Citation information: DOI 10.1109/TBCAS.2019.2917690, IEEE Transactions on Biomedical Circuits and Systems

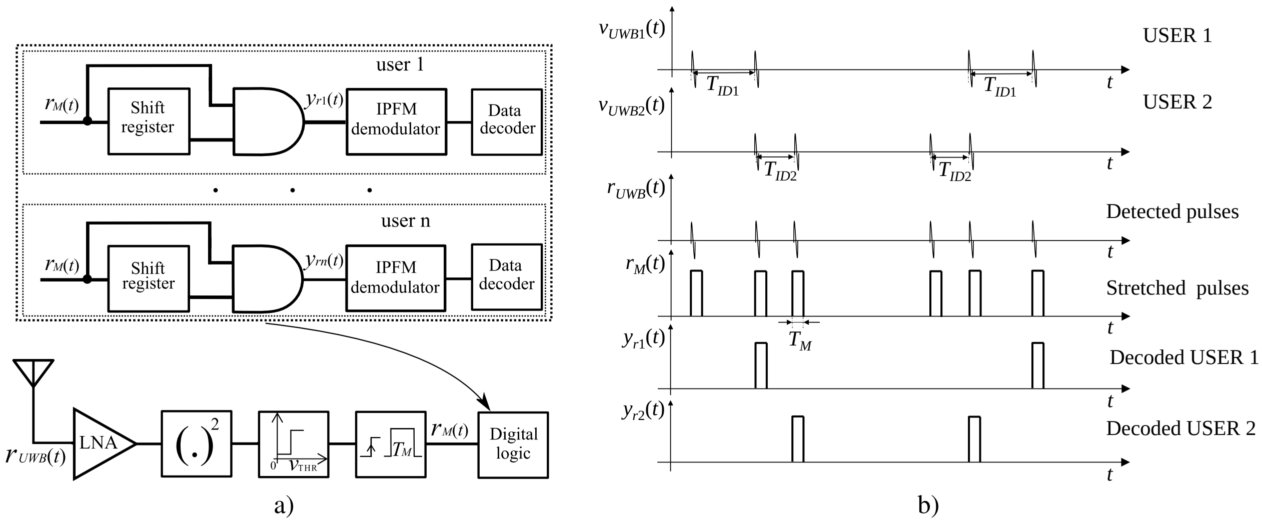

Fig. 6: Block scheme of the Time Encoding Ultra-Wideband a) receiver and b) corresponding pulse waveforms for the two user scenario.

Fig. 5 represents simulated waveforms $x(t)$, $y(t)$, $l_{INF}(t)$, $l_{ID}(t)$ and $v_{UWB}(t)$ for $x(t) = 0.35 + 0.2sin(6.28 \times 10^4 t)$. The sinusoidal input signal $x(t)$ is modulated to time information using the IPFM and two UWB pulses $v_{UWB}(t)$ are formed per each IPFM output pulse $y(t)$. The time distance between two UWB pulse pairs conveys the information on the input signal value, while the distance between UWB pulses within one UWB pulse pair (bottom waveform $v_{UWB}(t)$) is unique per particular user. Due to the asynchronous operation and low duty cycling of the output pulse train $y(t)$, the TE-UWB transmitter provides energy efficient multi-user analog to time conversion and wireless transmission. Therefore, it is a promising solution compared to standard analog-to-digital converters used for analog biosensor signal acquisition and wireless transmission. Since the TE-UWB transmitter implementation is predicted for unipolar power supply application, it also requires unipolar analog input signals. The input signal $x(t)$ can be provided by an analog biosensor with the unipolar analog voltage output.

Fig. 6a presents a block scheme of the TE-UWB receiver. It includes the UWB pulse detector and the pulse stretcher, which are drive the decoder and the demodulator in Digital logic block. The duration T_M of the pulse at the output of the pulse stretcher depends on the minimal pulse width limited by the Digital logic used for user decoding and signal demodulation. User decoding can be performed using analog asynchronous delay lines or counter-based time to digital converters, which affects the decoding and demodulation resolution. An example of the two-user transmission scenario receiver waveforms is provided in Fig. 6. Two users generate TE-UWB pulse streams sharing the same communication channel. The received UWB pulses $r_{UWB}(t)$ are stretched ($r_M(t)$) prior to decoding and demodulation in Digital logic. Delaying the pulse train $r_M(t)$ by a particular sensor ID time delay T_{ID} extracts the corresponding IPFM pulse train for a particular user (USER1 and USER2). Measurement results of the TE-UWB receiver decoding and demodulation performances, together with the Symbol Error Rate (SER), are analysed in [33]. Due to a low frequency range of biological signals, the proposed system provides efficient multi-sensor communication for up to 20 sensors within the same BAN. To obtain energy efficient wireless transmission, UWB communications have been recognized as suitable solution [34]–[36]. Since the value of the analog input signal applied to the TE-UWB transmitter is coded into the IPFM pulse distance and the sensor ID is coded into the IPFM pulse width, triggering the UWB pulse generator directly with IPFM pulse rising and falling edges, provides microprocessor and clock free coding and wireless transmission. Accordingly, TE-UWB multi-user coding is essentially comparable to transmitted-reference UWB (TR-UWB) systems. A transmitted-reference technique employs a delay cell to create a delayed replica of the original UWB pulse [37]–[39]. The reported contributions in the field of TR-UWB use synchronized pulse generation and coding, which is the major difference compared to TE-UWB. The introduced time-encoding concept enables a direct analog signal to time modulation, providing rectangular pulses for simple and energy efficient multi-user coding and wireless transmission. Delaying rectangular pulses is more simple, prevents spectrum degradation and provides lower energy consumption of the generated UWB pulses, compared to delaying ultra-wideband pulses directly.

III. TE-UWB TRANSMITTER IMPLEMENTATION

The implemented TE-UWB transmitter from Fig. 3 is designed and simulated in Cadence Virtuoso tools, using TSMC PDK for TSMC 180 nm CMOS technology. The total transmitter chip area is 0.14 mm^2. According to the implemented technology, the length of all transistors is equal to 180 nm, while the default transistor width is equal to 2 μm. In particular sub-circuits, several transistors have diverse widths defined in Table I.

The integrator $L_{INF}(s)$ is implemented by using the current source that charges capacitor C_1 with constant current I_{CINF} (Fig. 7) and enables charging (Reset pin is in logic "1") and

This article has been accepted for publication in a future issue of this journal, but has not been fully edited. Content may change prior to final publication. Citation information: DOI 10.1109/TBCAS.2019.2917690, IEEE Transactions on Biomedical Circuits and Systems

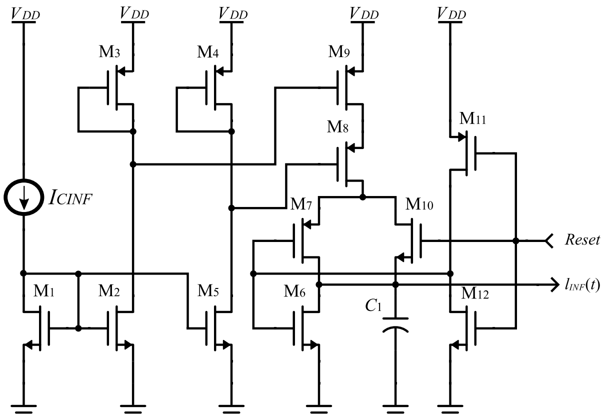

Fig. 7: Circuit implementation of the integrator $L_{INF}(s)$.

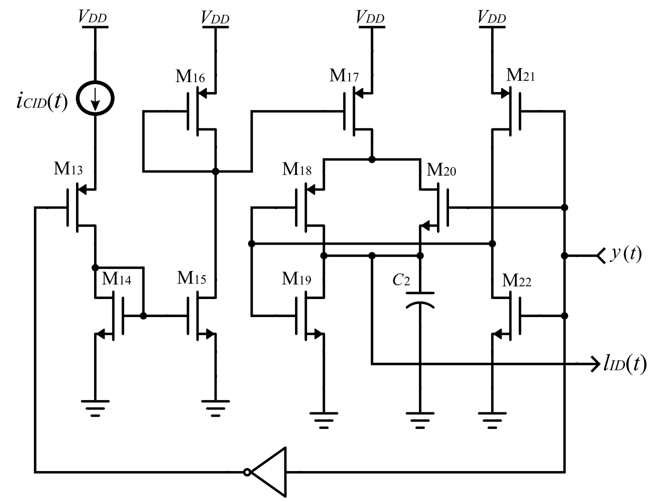

Fig. 8: Circuit implementation of the integrator $L_{ID}(s)$.

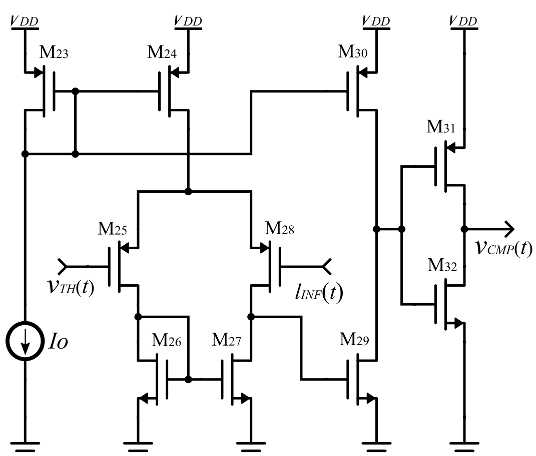

Fig. 9: Circuit implementation of the comparator.

fast discharging (Reset pin is in logic "0") of metal-insulator-metal (MIM) capacitor $C_1 = 1.79$ pF. To enable capacitor C_1 current control, the resistor is placed outside the IC for test purposes. Charging current I_{CINF} defines time constant τ_{INF} and significantly contributes to static power consumption of the TE-UWB transmitter. The integrator input voltage is set

TABLE I: Transistor widths

Transistor	Figure	Width, [μm]
M6	Fig. 7	6
M19	Fig. 8	6
M23	Fig. 9	4
M34	Fig. 10	10
M40	Fig. 10	5
M41	Fig. 10	3
M42	Fig. 10	10
M43	Fig. 10	8
M44	Fig. 10	75

to supply voltage $V_{DD} = 1.8$ V.

Fig. 8 presents integrator $L_{ID}(s)$ used for sensor ID generation. When the Q output of the SR latch is in logic "1" state, the capacitor $C_2 = 1.2$ pF is charged with the current source controlled by the current $i_{CID}(t)$. The capacitor is charged until the voltage $l_{ID}(t)$ reaches the inverter threshold $V_{DD}/2$ and resets the SR latch. To achieve a wide range of controllable T_{ID} delay values, a change in the τ_{ID} constant is performed by changing the value of the $i_{CID}(t)$ current with an external resistor. Because the integrator $L_{ID}(s)$ is most of the time in the off state, the inverter logic gate turns off the current mirror in that state to provide minimum power consumption.

To prevent faster $L_{INF}(s)$ setting ON before its capacitor C_1 is discharged to zero voltage, the SR latch is implemented in the feedback loop of the IPFM. It sets or resets the integrator according to the comparator output voltage $y(t)$ and the $L_{ID}(s)$ integrator output voltage peak. Comparator circuit implementation is depicted in Fig. 9. Due to advantages of the TSMC 180 nm CMOS process, the comparator provides high slew rates for rising and falling rectangular pulse edges, which is important for efficient UWB pulse generation. The circuit of the proposed UWB pulse shaper is presented in Fig. 10. The implemented UWB pulse shaper is an improved modification of the pulse generator from [40] and it provides improved pulse shaping according to the outdoor FCC spectrum mask. The circuit consists of three parts: I) a monostable multivibrator, II) a driver for the output MOSFET and III) an output shaping circuit. For $z(t) = 0$, the capacitor $C_3 = 1.79$ pF in III) is fully charged to voltage V_{DD} and inductor $L_1 = 1nH$ is discharged. When an impulse is formed at the output of the monostable circuit, it turns on the MOSFET M44 which discharges the capacitor C_{P1}, thus forming the negative Gaussian impulse at the input of the external pulse shaping filter in IV) (Fig. 10). At the same time, M44 drain current charges the inductor L_1. Once $z(t)$ becomes 0, the energy stored in the inductor is released through the external pulse shaping filter IV), forming the positive Gaussian impulse on the drain of the MOSFET M44. The sum of positive and negative Gaussian impulses forms the Gaussian monocycle impulse at the input of the external pulse shaping filter. On state duration of M44 is determined by the L_1/R_M time constant, where R_M is saturation resistance of M44. Further pulse shaping is performed in part IV) with the parasitic inductance of the bonding wire $L_{P1} = 4nH$, the parasitic capacitor of the

This article has been accepted for publication in a future issue of this journal, but has not been fully edited. Content may change prior to final publication. Citation information: DOI 10.1109/TBCAS.2019.2917690, IEEE Transactions on Biomedical Circuits and Systems

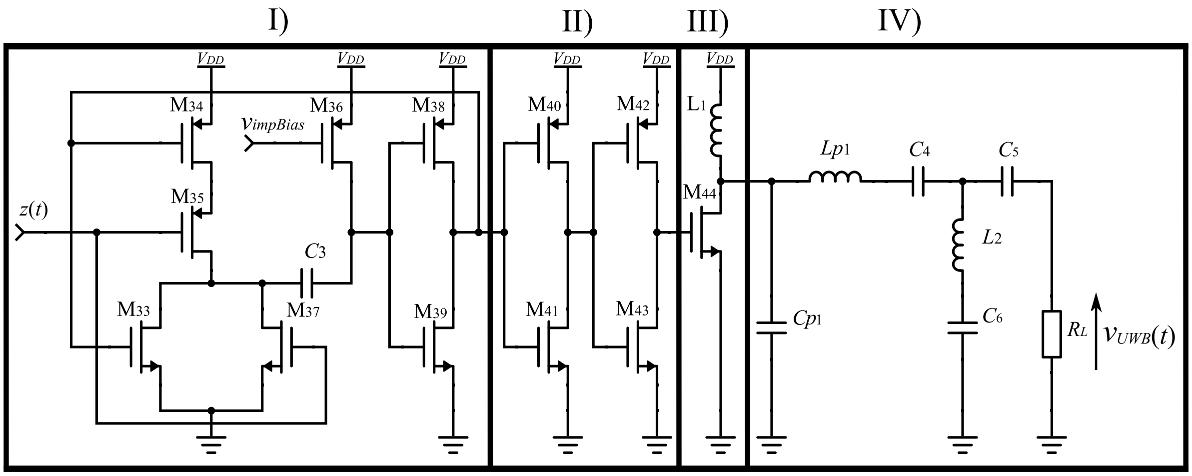

Fig. 10: Circuit implementation of the UWB pulse shaper with an external pulse shaping filter IV).

TABLE II: Standard deviation of IPFM output signal period $t_k - t_{k-1}$.

$x(t)$, [V]	0,15	0,25	0,35	0,45	0,55	0,65	0,75	0,85	0,95	1,05	1,15	1,25	1,35	1,45	1,55
$mean(t_k - t_{k-1})$, [μs]	1,87	3,09	4,21	5,36	6,52	7,69	8,89	10,11	11,33	12,57	13,87	15,12	16,43	17,91	20,28
σ, [ns]	5,44	5,26	5,94	8,13	9,22	9,81	11,35	13,07	14,9	15,72	19,34	19,84	20,3	22,46	24,63

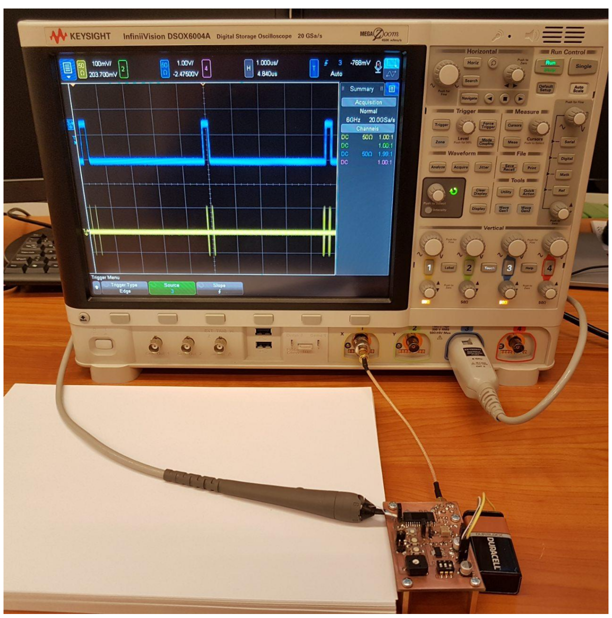

Fig. 11: Measurement setup for time domain measurement of $y(t)$ and $v_{UWB}(t)$ for $x(t) = 0.32$ V.

bonding pad, the analog 3.3V ESD cell $C_{P1} = 1$pF and the external pulse shaping filter ($L_2 = 6.8$nH, $C_6 = 3.3$pF, $C_4 = C_3 = 0.5$pF, $R_L = 50\Omega$). To reduce the impact of technological imperfections and temperature, the monostable multivibrator enables precise control of the impulse width by using the external voltage source $VimpBias$.

IV. Simulation and Measurement Results

The measurements of the pulse shape in time domain and jitter is performed with the Keysight DSOX6004A 20 GS/s oscilloscope, while its PSD is measured with the Anritsu MT8222A spectrum analyzer. Power consumption of the TE-UWB transmitter is measured using Keysight CX3324A current waveform analyser. Measurement setup for $y(t)$ and $v_{UWB}(t)$ time-domain measurement (for $x(t) = 320$ mV) is provided in Fig. 11. Upper trace presents IPFM output signal $y(t)$, while lower trace presents TE-UWB output signal $v_{UWB}(t)$. The same setup is used for IPFM output signal $y(t)$ cycle to cycle jitter measurement. Measurement results of the cycle to cycle jitter standard deviation σ and its dependence on the mean value of time distance between two consecutive IPFM output pulses $mean(t_k - t_{k-1})$ are provided in Fig. 12 and in Table II. Each value is obtained for 1000 samples per one measurement of σ value. According to the noise analysis for comparator-based circuits, provided in [41], the dominant source of the noise in the proposed IPFM circuit is a jitter at the output of the comparator, caused by the noisy current source which charges capacitor C_1 whose voltage feeds the input of the comparator. Due to the higher flicker noise corner frequency, comparing to the IPFM output pulse train frequency, a flicker noise is dominant. Therefore, the jitter

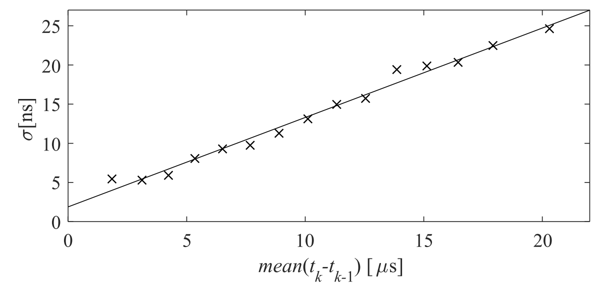

Fig. 12: Standard deviation of IPFM output signal period $t_k - t_{k-1}$.

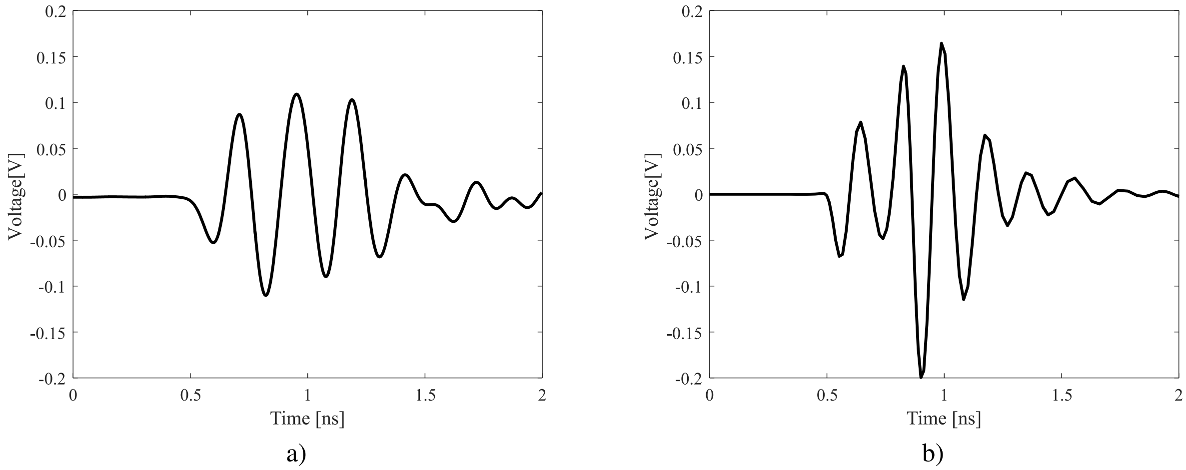

Fig. 13: Output UWB pulse waveform a) measured and b) simulated.

standard deviation σ is rising with the IPFM output signal period $t_k - t_{k-1}$ for entire voltage measurement range. The simulated and measured IR-UWB pulse $v_{UWB}(t)$ in time domain is shown in Fig. 13. To maintain the UWB pulse shape independent of the parasitic influence to the UWB pulse generator and shaper, the monostable multivibrator biasing voltage is adjusted by setting $V_{impBias}$ to 926 mV.

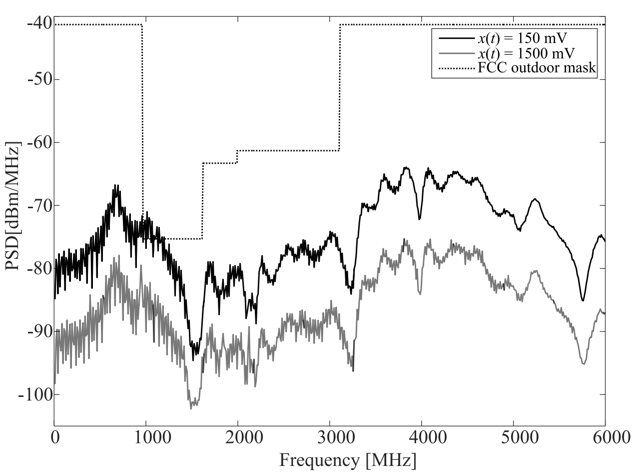

Fig. 14: Power spectral density of the UWB pulse train for $x(t)$ = 0.15 V and $x(t)$ = 1.5 V

Generated UWB pulse waveform time domain measurement and simulation results are presented in Fig. 13. The measured pulse achieves a peak-to-peak amplitude equal to $240\ mV$ with 1ns envelope (Fig. 13a), while a simulated pulse achieves a $350\ mV$ peak-to-peak amplitude with equal envelope width. The power spectral densities of the measured UWB pulses are provided in Fig. 14. The simulated pulse has a higher amplitude and a slightly different shape due to the mismatch of the simulated and real values of parasitic components. The black and the gray trace represent the measured PSD for the modulation signal $x(t) = 0.15$ V and $x(t) = 1.5$ V, respectively. For higher values of the analog input signal $x(t)$, the transmitter achieves lower pulse repetition frequencies, which in turn provides lower power spectral densities, like on the gray trace in Fig. 14. Due to the low pulse repetition rate, the power spectral density is far below the allowed limits according to the FCC outdoor mask requirements. The low power spectral density enables application of output power amplifiers and a higher output voltage swing for wireless transmission range extension, since the communication distance depends on the impulse amplitude. The power spectral density is affected by the pulse repetition rate, which in turn depends on the input signal level. The pulse repetition rate can also be affected by changing the integrator time constant/gain.

TABLE III: Estimated power consumption for biological signal acquisition

Biomedical signal	**Frequency range, [Hz]**	**Maximal power consumption for $OSR = 100$, [μW]**
Action Potential	100 - 2000	20.43
Electroneurogram (ENG)	100 - 1000	16.26
Surface Electromyogram (SEMG)	2 - 500	13.13
Electroencephalogram (EEG)	0.5 - 100	10.63
Electrocardiogram (ECG)	0.05 - 100	10.63

Total simulated power consumption of the TE-UWB transmitter for the minimum DC input voltage is $40.48\ \mu$W, while the supply current is equal to $22.49\ \mu$A. For the maximum DC input voltage, total power consumption wanes to 10.80 μW, while the supply current is equal to $6\ \mu$A. The IPFM transfer function with corresponding TE-UWB transmitter power consumption is provided in Fig. 15a, while Fig. 15b presents the dependence of total power consumption P on the time distance between two consecutive pulse pairs $t_k - t_{k-1}$. The transfer function of the IPFM transmitter is defined as the dependence of time distance between two consecutive pulse pairs $t_k - t_{k-1}$ on the analog input voltage instantaneous value $x(t)$. According to equation (10), time distance between two

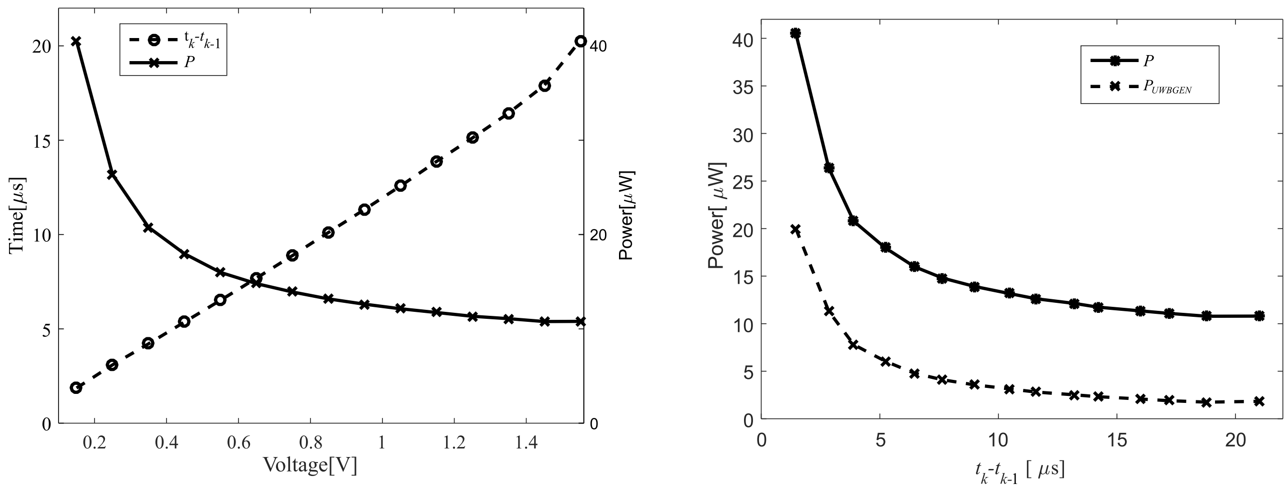

a) b)

Fig. 15: IPFM a) transfer function with corresponding TE-UWB transmitter power consumption and b) dependence of power consumption P on the two consecutive pulse distance $t_k - t_{k-1}$.

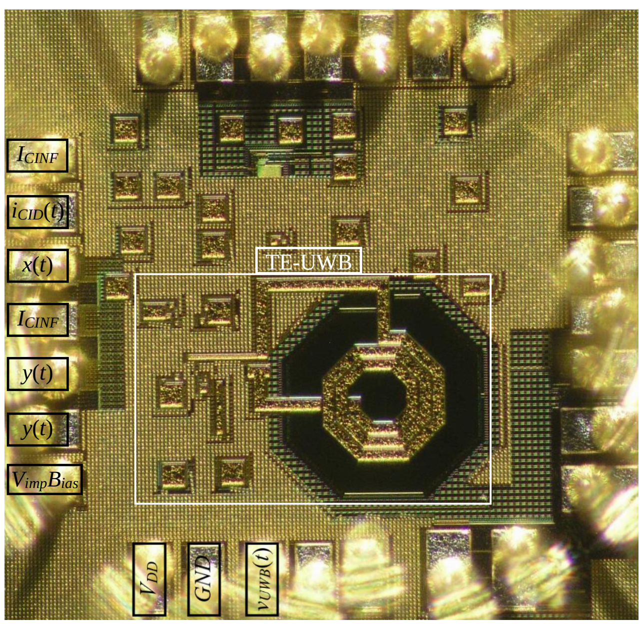

Fig. 16: Die photo of the implemented TE-UWB transmitter.

consecutive pulse pairs distance $t_k - t_{k-1}$ is proportional to the $L_{INF}(s)$ integrator time constant τ_{INF}. Therefore, for the constant input voltage $x(t)$, power consumption can be further reduced by increasing the time constant τ_{INF}. Since the bandwidth ω of the analog input signal $x(t)$ is limited to satisfy the condition $1/\tau_{INF} >> \omega$, depending on its value and the fixed oversampling ratio OSR, which can be defined as

$$OSR = \frac{1}{\max(t_k - t_{k-1})\max(\omega)}, \tag{11}$$

estimated average power consumption can be calculated for application specific wireless acquisition of biological signals. Maximal power consumption can be obtained by integrating the power consumption curve (Fig. 15b) over the entire $t_k - t_{k-1}$ span and calculating its mean value. For fixed $OSR = 100$, estimated maximal power consumption of the TE-UWB transmitter for various biological signals [23] with their corresponding frequency range is provided in Table III. Despite non-uniform frequency spectrum distribution of various biological signals, to ensure proper time encoding, OSR is defined according to the highest frequency spectral component of the measured signal (11). Additionaly, for each spectral component, maximal input signal amplitude is assumed. Therefore, maximal power consumption estimated in Table III is a worst-case scenario predicted for proper modulation of highest frequency component. For sparse signals and a non-uniform frequency spectrum, like ECG signal spectrum [42], power consumption could be further reduced. This would, however require implementation of adaptive TEM modulation techniques and dynamic OSR change. According to the properties of the proposed TE-UWB transmitter, the power consumption rises for shorter time distances between two consecutive pulse pairs $t_k - t_{k-1}$. Due to a highest frequency range, measurement of the Action Potential requires a higher IPFM pulse repetition frequency and therefore it would consume more power compared to the signals with a lower frequency range, like EEG or ECG. For low input signal bandwidths, lower power consumption can be achieved, maintaining the same OSR. For biological signals with lower frequency bands, due to low duty cycling operation, average power consumption tends to static power consumption.

According to the provided state-of-the-art, the time encoded multi-user system for continuous monitoring comparable to the proposed TE-UWB transmitter has not been published so far. Due to asynchronous modulation, it is not straightforwardly comparable with competing short range communication systems in terms of Bit-Error-Rate and due to the power consumption dependence on the input signal level, it is also difficult to compare its power consumption with competing solutions.

This article has been accepted for publication in a future issue of this journal, but has not been fully edited. Content may change prior to final publication. Citation information: DOI 10.1109/TBCAS.2019.2917690, IEEE Transactions on Biomedical Circuits and Systems

TABLE IV: Summary of the TE-UWB performances and comparison with the state-of-the-art transmitters

Source	**Techn.,** [nm]	**Modulation**	**Method**	**Analog input**	**Multi-user functionality**	**Frequency Band,** [GHz]	**Data rate,** [Mbps]	**Pulse amplitude,** [mV]	**Energy,** [pJ/b]	**Area,** [mm^2]	**Power consumption,** [μW]
This work	180	IPFM	Edge combining	Yes	Yes	3.5 - 5.5	0.5[a]	120	80	0.14	40.48[b] 19.98[c]
MWCL '18 [1]	65	OOK	Edge combining	No	No	3.1 - 4.1	200	110	4.32	0.065	0.86
TCAS-II '18 [3]	180	OOK	LO-based	No	No	3.1 - 6	200	130	20	0.021	4000
TCAS-II '16 [25]	180	Time encoding	Edge combining	Yes[d]	No	3 - 5.1	0.05	650	75	3.89	3.75
TBCAS '16 [34]	180	OOK	Edge combining	No	No	3.1 - 7	500	75	7	0.01	3500
TCAS-I '18 [35]	130	OOK	Direct, Double PLL	No	No	3.5 - 4.5	1000	50	5	0.04	5000
JSSC '14 [36][e]	130	OOK	Edge combining	Yes	Yes	0 - 1, 3 - 10.6	0.09[e]	90	758	0.08[f]	68[e]

[a]Obtained for a 1-bit digital input signal. [b]Including the IPFM. [c]Excluding the IPFM. [d]Physical value. [e]Per channel. [f]One channel + UWB transmitter.

However, according to the presented results, a comparison with the most relevant IR-UWB transmitters is provided in Table IV. The proposed TE-UWB transmitter is designed to enable wireless acquisition of analog input signals, including IPFM analog voltage to time conversion, multi-user coding and UWB wireless transmission. However, it can be applied for 1-bit digital input signals and for such signals it is comparable to IR-UWB transmitters [1], [3], [34], [35] from Table IV. Despite the low data rate compared to transmitters in the references [1], [3], [33], [34], the fact that the TE-UWB output pulse pair distance contains analog information on the input signal $x(t)$, for high OSR values (for slowly varying input signals) time distance between two consecutive pulse pairs $t_k - t_{k-1}$ contains the entire symbol value. Accordingly, transmitting four TE-UWB pulse pairs provides multi-user coded multi-bit information. However, for single-user operation and a 1-bit digital input signal, the TE-UWB transmitter can be implemented without the IPFM, which significantly reduces power consumption. Fig. 15b presents the power consumption dependence on time distance between two consecutive pulse pairs $t_k - t_{k-1}$ for the transmitter with the IPFM (solid line - P) and without the IPFM (dashed line P_{UWBGEN}). Excluding the IPFM modulator reduces power consumption of the entire TE-UWB transmitter in 20.5μW for high pulse repetition rates. Comparing to [25], TE-UWB provides multi-user coding, while it consumes slightly higher energy per transmitted bit. Also, unlike the transmitter in [25], it can be used as a wireless transmitter for acquisition of any type of a measured analog biomedical signal. The IR-UWB transmitter reported in [36] is the closest prior art transmitter enabling multi-user transmission and the analog signal input. However, it provides a lower data rate per channel and consumes more energy. Conclusively, the major benefit of the proposed transmitter is simple and energy efficient multi-user coding which consumes less power comparing to transmitter reported in [36] and does not imply significantly higher power consumption comparing to the other single-user UWB transmitters reported in Table IV. Therefore, TE-UWB transmitter, proposed in this work brings additional advantage of multi-user operation for the price of increment in power consumption. Additional benefits of the TE-UWB transmitter and reference [25] comparing to the other state-of-the-art transmitters are asynchronous operation and more simple receiver design which does not require synchronisation. The plot of the implemented IC is provided in Fig. 16 with a highlighted transmitter area.

V. Conclusions

The paper presents a novel implementation of the TE-UWB transmitter for wireless sensing applications in 180 nm CMOS technology. The transmitter architecture is based on TEM analog to time conversion and UWB pulse wireless transmission. IPFM application provides linear dependence of the analog input voltage to the IPFM output pulse distance. Also, the IPFM enables unipolar pulse operation, which enables energy efficiency for unipolar input signal applications. Multi-sensor application is achieved by delay-based multi-user coding. Each sensor exhibits unique time delay denoted as the sensor ID, which is used for particular sensor decoding on the receiver side. Due to delay-based coding, neither microprocessor nor clock signal is needed on the transmitter side, which enables energy efficient operation for constant monitoring applications. Constant monitoring is required in numerous biomedical wireless sensing applications. Therefore, the proposed architecture enables a wide range of application areas for BAN short range wireless connectivity. Compared to the multi-channel UWB transmitter in [36], the proposed TE-UWB transmitter provides lower power consumption. With respect to the state-of-the-art single-user UWB transmitters, for the price of slightly higher power consumption, it provides multi-user communication. The advantage of the proposed system is asynchronous operation, which eliminates demand for synchronisation on the receiver side. It can be implemented by using a sliding correlator or a simple level detector.

This article has been accepted for publication in a future issue of this journal, but has not been fully edited. Content may change prior to final publication. Citation information: DOI 10.1109/TBCAS.2019.2917690, IEEE Transactions on Biomedical Circuits and Systems

REFERENCES

[1] Y. Lin, S. Park, X. Chen, D. Wentzloff, and E. Yoon, "4.32-pj/b, overlap-free, feedforward edge-combiner-based ultra-wideband transmitter for high-channel-count neural recording," *IEEE Microwave and Wireless Components Letters*, vol. 28, no. 1, pp. 52–54, Jan 2018.

[2] H. Ando, K. Takizawa, T. Yoshida, K. Matsushita, M. Hirata, and T. Suzuki, "Wireless multichannel neural recording with a 128-mbps uwb transmitter for an implantable brain-machine interfaces," *IEEE Transactions on Biomedical Circuits and Systems*, vol. 10, no. 6, pp. 1068–1078, Dec 2016.

[3] K. Ture, A. Devos, F. Maloberti, and C. Dehollain, "Area and power efficient ultra-wideband transmitter based on active inductor," *IEEE Transactions on Circuits and Systems II: Express Briefs*, vol. 65, no. 10, pp. 1325–1329, Oct 2018.

[4] S. Sapienza, M. Crepaldi, P. M. Ros, A. Bonanno, and D. Demarchi, "On integration and validation of a very low complexity atc uwb system for muscle force transmission," *IEEE Transactions on Biomedical Circuits and Systems*, vol. 10, no. 2, pp. 497–506, April 2016.

[5] R. Bharadwaj, S. Swaisaenyakorn, C. G. Parini, J. C. Batchelor, and A. Alomainy, "Impulse radio ultra-wideband communications for localization and tracking of human body and limbs movement for healthcare applications," *IEEE Transactions on Antennas and Propagation*, vol. 65, no. 12, pp. 7298–7309, Dec 2017.

[6] X. Zhang, Z. Zhang, Y. Li, C. Liu, Y. X. Guo, and Y. Lian, "A 2.89μw dry-electrode enabled clockless wireless ecg soc for wearable applications," *IEEE Journal of Solid-State Circuits*, vol. 51, no. 10, pp. 2287–2298, Oct 2016.

[7] E. Schires, P. Georgiou, and T. S. Lande, "Vital sign monitoring through the back using an uwb impulse radar with body coupled antennas," *IEEE Transactions on Biomedical Circuits and Systems*, vol. 12, no. 2, pp. 292–302, April 2018.

[8] P. Park and S. Kim, "A continuous sweep-clock-based time-expansion impulse-radio radar," *IEEE Transactions on Circuits and Systems I: Regular Papers*, vol. 65, no. 9, pp. 3049–3059, Sep 2018.

[9] N. Decarli, F. Guidi, and D. Dardari, "Passive uwb rfid for tag localization: Architectures and design," *IEEE Sensors J.*, vol. 16, no. 5, pp. 1385–1397, March 2016.

[10] E. Nemati, M. J. Deen, and T. Mondal, "A wireless wearable ecg sensor for long-term applications," *IEEE Commun. Mag*, vol. 50, no. 1, pp. 36–43, Jan 2012.

[11] J. Andreu-Perez, D. R. Leff, H. M. D. Ip, and G. Z. Yang, "From wearable sensors to smart implants- x2013; toward pervasive and personalized healthcare," *IEEE Trans. Biomed. Eng.*, vol. 62, no. 12, pp. 2750–2762, Dec 2015.

[12] J. Wang, T. Fujiwara, T. Kato, and D. Anzai, "Wearable ecg based on impulse-radio-type human body communication," *IEEE Trans. Biomed. Eng.*, vol. 63, no. 9, pp. 1887–1894, Sept 2016.

[13] A. Alderson, "Sports tech - wearable sensors [technology rugby]," *Engineering Technology*, vol. 11, no. 6, pp. 76–77, July 2016.

[14] M. R. Ebling, "Iot: From sports to fashion and everything in-between," *IEEE Pervasive Comput*, vol. 15, no. 4, pp. 2–4, Oct 2016.

[15] G. E. Santagati and T. Melodia, "A software-defined ultrasonic networking framework for wearable devices," *IEEE/ACM Trans. Netw*, vol. 25, no. 2, pp. 960–973, April 2017.

[16] F. Li, J. Luo, G. Shi, and Y. He, "Art: Adaptive frequency-temporal co-existing of zigbee and wifi," *IEEE Trans. Mobile Comput*, vol. 16, no. 3, pp. 662–674, March 2017.

[17] A. Paidimarri, N. Ickes, and A. P. Chandrakasan, "A +10 dbm ble transmitter with sub-400 pw leakage for ultra-low duty cycles," *IEEE J. Solid-State Circuits*, vol. 51, no. 6, pp. 1331–1346, June 2016.

[18] H. Jiang, Y. Guo, Z. Wu, C. Zhang, W. Jia, and Z. Wang, "Implantable wireless intracranial pressure monitoring based on air pressure sensing," *IEEE Transactions on Biomedical Circuits and Systems*, vol. 12, no. 5, pp. 1076–1087, Oct 2018.

[19] H. Bhamra, J. Tsai, Y. Huang, Q. Yuan, J. V. Shah, and P. Irazoqui, "A subcubic millimeter wireless implantable intraocular pressure monitor microsystem," *IEEE Transactions on Biomedical Circuits and Systems*, vol. 11, no. 6, pp. 1204–1215, Dec 2017.

[20] F. Xu, G. Yan, K. Zhao, L. Lu, J. Gao, and G. Liu, "A wireless capsule system with asic for monitoring the physiological signals of the human gastrointestinal tract," *IEEE Transactions on Biomedical Circuits and Systems*, vol. 8, no. 6, pp. 871–880, Dec 2014.

[21] A. F. Yeknami, X. Wang, I. Jeerapan, S. Imani, A. Nikoofard, J. Wang, and P. P. Mercier, "A 0.3-v cmos biofuel-cell-powered wireless glucose/lactate biosensing system," *IEEE Journal of Solid-State Circuits*, vol. 53, no. 11, pp. 3126–3139, Nov 2018.

[22] C. J. Lukas, F. B. Yahya, J. Breiholz, A. Roy, X. Chen, H. N. Patel, N. Liu, A. Kosari, S. Li, D. Akella Kamakshi, O. Ayorinde, D. D. Wentzloff, and B. H. Calhoun, "A 1.02 µw battery-less, continuous sensing and post-processing sip for wearable applications," *IEEE Transactions on Biomedical Circuits and Systems*, vol. 13, no. 2, pp. 271–281, April 2019.

[23] J. D. Bronzino, *The Biomedical Engineering HandBook, Second Edition*. CRC Press LLC, 2000.

[24] H. Liu, J. Sarrazin, F. Deshours, T. Mavridis, L. Petrillo, Z. Liu, P. D. Doncker, and A. Benlarbi-Delaï, "Performance assessment of ir-uwb body area network (ban) based on ieee 802.15.6 standard," *IEEE Antennas Wireless Propag. Lett.*, vol. 15, pp. 1645–1648, 2016.

[25] J. Mao, Z. Zou, and L. R. Zheng, "A uwb-based sensor-to-time transmitter for rf-powered sensing applications," *IEEE Trans. Circuits Syst. II, Exp. Briefs*, vol. 63, no. 5, pp. 503–507, May 2016.

[26] A. A. Lazar and L. T. Toth, "Time encoding and decoding of a signal," Aug 2009, US Patent 7,573,956.

[27] S. Ouzounov, E. Roza, J. A. Hegt, G. van der Weide, and A. H. M. van Roermund, "Analysis and design of high-performance asynchronous sigma-delta modulators with a binary quantizer," *IEEE J. Solid-State Circuits*, vol. 41, no. 3, pp. 588–596, March 2006.

[28] T. Matić, M. Herceg, J. Job, and L. Šneler, "Ultra-wideband transmitter based on integral pulse frequency modulator," in *Proc. 2016 MIPRO*, May 2016, pp. 80–83.

[29] ——, "The receiver circuit for ultra-wideband integral pulse frequency modulated wireless sensor," in *Proc. 2016 MOCAST)*, May 2016, pp. 1–4.

[30] T. Matic, M. Herceg, and J. Job, "Energy-efficient system for distant measurement of analog signals," Dec 2014, WO/2014/195739.

[31] ——, "Energy-efficient system for distant measurement of analog signals," Dec 2014, WO/2014/195744.

[32] S. Naraghi, M. Courcy, and M. P. Flynn, "A 9-bit, 14 µW and 0.06 mm^2 pulse position modulation adc in 90 nm digital cmos," *IEEE J. Solid-State Circuits*, vol. 45, no. 9, pp. 1870–1880, Sept 2010.

[33] L. Sneler, T. Matic, and I. Galic, "The fpga system for evaluation of uwb wireless sensor network based on transmitted reference integral pulse frequency modulator," in *2018 Zooming Innovation in Consumer Technologies Conference (ZINC)*, May 2018, pp. 55–57.

[34] S. A. Mirbozorgi, H. Bahrami, M. Sawan, L. A. Rusch, and B. Gosselin, "A single-chip full-duplex high speed transceiver for multi-site stimulating and recording neural implants," *IEEE Transactions on Biomedical Circuits and Systems*, vol. 10, no. 3, pp. 643–653, June 2016.

[35] M. Crepaldi, G. N. Angotzi, A. Maviglia, F. Diotalevi, and L. Berdondini, "A 5 pj/pulse at 1-gpps pulsed transmitter based on asynchronous logic master–slave pll synthesis," *IEEE Transactions on Circuits and Systems I: Regular Papers*, vol. 65, no. 3, pp. 1096–1109, March 2018.

[36] H. M. Jafari, K. Abdelhalim, L. Soleymani, E. H. Sargent, S. O. Kelley, and R. Genov, "Nanostructured cmos wireless ultra-wideband label-free pcr-free dna analysis soc," *IEEE Journal of Solid-State Circuits*, vol. 49, no. 5, pp. 1223–1241, May 2014.

[37] X. Luo and G. B. Giannakis, "Achievable rates of transmitted-reference ultra-wideband radio with ppm," *IEEE Trans. Commun.*, vol. 54, no. 9, pp. 1536–1541, Sept 2006.

[38] D. I. Kim and T. Jia, "M-ary orthogonal coded/balanced ultra-wideband transmitted-reference systems in multipath," *IEEE Trans. Commun.*, vol. 56, no. 1, pp. 102–111, Jan 2008.

[39] D. J. J. A. Ekbal, C. U. Lee, "Rate division multiple access for uwb systems," May 2008, WO2008061245 A2.

[40] L. Šneler, M. Herceg, and T. Matić, "Ultra-wideband pulse generator for time-encoding wireless transmission," in *Proc. 2017 MIPRO*, May 2017, pp. 109–112.

[41] T. Sepke, P. Holloway, C. G. Sodini, and H. Lee, "Noise analysis for comparator-based circuits," *IEEE Transactions on Circuits and Systems I: Regular Papers*, vol. 56, no. 3, pp. 541–553, March 2009.

[42] N. V. Thakor, "From holter monitors to automatic defibrillators: Developments in ambulatory arrhythmia monitoring," *IEEE Transactions on Biomedical Engineering*, vol. BME-31, no. 12, pp. 770–778, Dec 1984.

Tomislav Matić received the M.Sc. and Ph.D. degrees in electrical engineering from the Faculty of Electrical Engineering, Computer Science and Information Technology Osijek, University of Osijek, Croatia, in 2002 and 2010, respectively. He is currently Associate Professor at the Department of Communications, Faculty of Electrical Engineering, Computer Science and Information Technology Osijek.

His research interests include analog-to-digital conversion, time encoding, asynchronous circuits design, ultra-wideband systems, wireless communications and biomedical circuits and systems. He is a member of IEEE Circuits and Systems Society, IEEE Solid-State Circuits Society and IEEE Engineering in Medicine and Biology Society.

Leon Šneler received his B.Sc. and M.Sc. degree in electrical engineering from Faculty of Electrical Engineering, Computer Science and Information Technology, Osijek, Croatia in 2011 and 2013, respectively. He is currently pursuing the Ph.D. degree in electrical engineering at the Faculty of Electrical Engineering, Computer Science and Information Technology Osijek. From 2016 he is a Research assistant at project “Energy efficient asynchronous wireless transmission” funded by the Croatian Science Foundation.

His research interest includes low power, RF and UWB analog IC design, time encoding, ultra-wideband communication systems, RTL-design, embedded systems, and low power wireless circuits.

Marijan Herceg received the B.Sc. and Ph.D. degrees in Electrical Engineering from the Faculty of Electrical Engineering, Computer Science and Information Technology Osijek, Croatia, in 2002 and 2010, respectively. He is currently an Associate Professor at the Department of Communications, Faculty of Electrical Engineering, Computer Science and Information Technology Osijek, Croatia.

His research interests include advanced modulation techniques, multiple access techniques, biomedical electronics, and sigma-delta A/D converters. He is a reviewer for several IEEE journals and a member of IEEE Communications Society.